



<http://www.diva-portal.org>

Postprint

This is the accepted version of a paper published in *Journal of Physical Chemistry Letters*. This paper has been peer-reviewed but does not include the final publisher proof-corrections or journal pagination.

Citation for the original published paper (version of record):

Liu, J., Roberts, M., Younesi, R., Dahbi, M., Edström, K. et al. (2013)
Accelerated Electrochemical Decomposition of Li₂O₂ under X-ray Illumination.
Journal of Physical Chemistry Letters, 4(23): 4045-4050
<http://dx.doi.org/10.1021/jz402230s>

Access to the published version may require subscription.

N.B. When citing this work, cite the original published paper.

Permanent link to this version:

<http://urn.kb.se/resolve?urn=urn:nbn:se:uu:diva-214019>

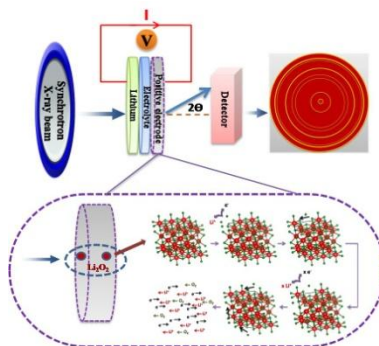
Accelerated electrochemical decomposition of Li_2O_2 under X-ray illumination

*Jia Liu, Matthew Roberts, Reza Younesi, Mohammed Dahbi, Kristina Edström, Torbjörn
Gustafsson, and Jiefang Zhu**

Department of Chemistry-Ångström Laboratory, Uppsala University, Box 538, SE-751 21
Uppsala, Sweden

ABSTRACT: This work presents the first report detailing the effect of X-rays on the electrochemical decomposition of Li_2O_2 , which is the main reaction during the charging process in a Li- O_2 battery. An *operando* synchrotron radiation powder X-ray diffraction (SR-PXD) experiment was performed. The results indicate that the electrochemical decomposition of Li_2O_2 is dramatically accelerated under X-ray irradiation. The accelerated decomposition of Li_2O_2 follows a zero-order reaction, and the decomposition rate constant is proportional to the intensity of X-ray used. A mechanism for the electrochemical decomposition of Li_2O_2 under X-ray irradiation is proposed. These results give an insight into the charging process in Li- O_2 batteries.

TOC GRAPHICS



KEYWORDS: Li- O_2 battery, synchrotron-based X-ray diffraction, fast charging, *operando* measurement, photoelectric effect, photoelectrochemistry, light-assisted electrochemical etching

In 1839, the photoelectric effect was first discovered by Becquerel who found that current could be generated without any external potential when AgCl was placed in an acidic solution and illuminated while connected to a Pt electrode. In the 1950's, researchers at Bell Labs began to study the possible use of photo-electrochemical effects to convert solar energy into electric power.¹ In 1972, Fujishima and Honda first reported that UV light irradiation enhanced the electrochemical decomposition of water using TiO₂ as a photocatalyst.² Their work triggered a rapid development of the photo-electrochemical cell. Many fundamental and applied advances have to day been achieved in the fields of environment and energy.³⁻⁴ In those photo-electrochemical systems, the photoactive material as a charge carrier plays a catalytic role in the reaction, and its composition does not change after each cycle of interactions. Equally, photo energy can directly speed up the electrochemical transformation of target materials, which means the substance can be electrochemically decomposed or generated under electromagnetic irradiation. UV or visible light has shown some applications in this field.⁵ However, the use of X-rays as a special light source has not been reported in the electrochemical transformation of solid materials.

The electrochemical decomposition of Li₂O₂ is the charging reaction in a non-aqueous Li-O₂ battery, which largely influences the charging rate, overpotential and rechargeability of the system.⁶ Besides several issues like instability of electrolytes,⁷⁻⁹ poor performance of lithium metal anode,¹⁰⁻¹¹ etc., one challenge for the Li-O₂ battery is to increase the kinetics of the electrode reaction, especially for the charging process.¹² Another conundrum is that the decomposition mechanism of Li₂O₂ is not yet clear.¹³ X-ray diffraction (XRD) has been applied as a simple, useful and direct measurement to investigate the formation and decomposition of Li₂O₂ for various designs of Li-O₂ battery.¹⁴⁻¹⁸ However, the low scattering ability of lithium and

oxygen and the limited X-ray intensity of normal in house diffractometers have led to a low sensitivity in Li_2O_2 detection. Synchrotron-based XRD offers several orders of magnitude higher X-ray intensity, much larger emitted X-ray spectrum, and a better resolution than a conventional research laboratory scale device. To the best of our knowledge, this powerful tool has been utilized only few times thus far in Li- O_2 battery research.¹⁹⁻²¹

Here, we investigated the influence of X-ray irradiation on the electrochemical decomposition of Li_2O_2 in a cell with propylene carbonate (PC) electrolyte, Li and porous Li_2O_2 -based electrodes. Synchrotron radiation powder X-ray diffraction (SR-PXD) was used both as a continuous X-ray source to advance the electrochemical decomposition of Li_2O_2 and an *operando* tool to quantify the rate of Li_2O_2 decomposition. The effect of X-ray intensity on the charging process of the Li_2O_2 -based cell was also investigated. This work provides a direct evidence of the acceleration of the electrochemical reactions by X-ray irradiation. In addition, fundamental information about the limiting factor and involved steps in Li_2O_2 electrochemical decomposition is revealed. Finally, to the best of our knowledge, this is the first report of X-ray irradiation being linked to effects on the electrochemical transformation of solid materials.

Li- O_2 cell components

The Li- O_2 cells were assembled using coffee bags with the following components: Li foil negative electrode, double-layer Solupor separator soaked in electrolyte (1 M LiPF_6 in PC), and porous Li_2O_2 -based positive electrode. It has been reported that the intermediate superoxide species formed during the discharge reaction (Oxygen Reduction Reaction (ORR)) of a Li- O_2 cell results in the decomposition of PC-based electrolytes.^{8-9, 22-24} However, since i) we only tested our cells during a charging process (OER); and ii) the oxidation potential of PC is higher than that of ether electrolytes,^{9, 25} PC electrolyte was considered suitable for this work.

The effect of X-ray irradiation on the decomposition of Li_2O_2 during the charging process of a Li-O₂ cell

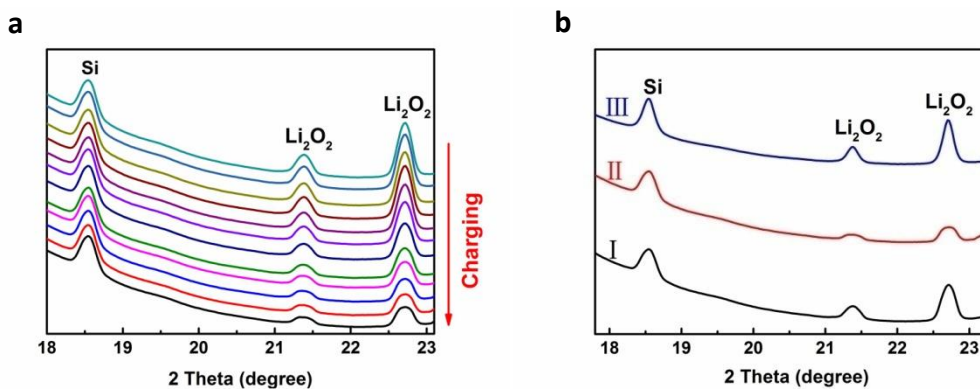


Figure 1.(a) The *operando* SR-PXD patterns of a Li_2O_2 -based electrode collected every 10 min during the charging at a constant current, and (b)The SR-PXD patterns of a Li_2O_2 -based electrode (I) before charging, after 3 h of charging at a constant current on a spot (II) with X-ray irradiation, and (III) without X-ray irradiation.

Fig. 1(a) shows a stacked plot of intensity vs. 2 theta collected for a Li_2O_2 -based electrode under continuous X-ray irradiation during charging at a constant current of $40 \text{ mA}\cdot\text{g}^{-1}$. Si (JCPDS File No: 04-014-0211) and Li_2O_2 (JCPDS File No: 04-013-3506) crystal phases were clearly observed. The absolute intensity of the Si reference peak decreased slightly as the intensity of synchrotron beam gradually faded during the measurement. However, the decrease in the intensity of the Li_2O_2 peaks is much more rapid, which confirms that the Li_2O_2 decomposition occurred during the charging process. The residual ratio of Li_2O_2 reduced to 49% after 110 minutes of charging. Qiao et al. reported that Li_2O_2 could be decomposed to Li_2O due to soft X-ray beam damage.²⁶ However, in our control experiment, while no charging current was applied to a cell containing the same amount of Li_2O_2 , there is little change in the amount of Li_2O_2 under constant X-ray irradiation for 8 hours (Fig. S1 in Supporting Information (SI)),

which indicates that the Li_2O_2 degradation observed in our work cannot simply be assigned to X-ray beam damage. In addition, the Li_2O peaks (JCPDS File No: 00-012-0254) were not observed in any collected pattern during continuous X-ray irradiation. In order to distinguish the effect of X-ray irradiation, an identical charging experiment was performed on a matching Li_2O_2 electrode, however, in the absence of constant X-ray irradiation. *In situ* XRD patterns of the electrode were collected at the start and end of the charging process (Fig. S2 in SI). The result showed that in the absence of an intense X-ray irradiation, the electrochemical decomposition of Li_2O_2 ran much slower than that under the X-ray irradiation. Therefore, it can be concluded that the X-ray irradiation does accelerate the electrochemical decomposition of Li_2O_2 .

To clarify this effect further, a Li_2O_2 -based electrode was charged for 3 h under constant X-ray irradiation on a single spot (0.8 mm diameter). Fig. 1(b) shows the SR-PXD patterns of a Li_2O_2 -based electrode before the charging, after 3 h of charging with X-ray irradiation, and without X-ray irradiation by moving the XRD measurement spot approximately 2 mm away from the irradiation spot on the same cell. Under continuous illumination, the Li_2O_2 peaks in Fig. 1(b, II) can be seen to have an obvious decrease in the intensity as compared to those peaks in the as prepared cell in Fig. 1(b, I). The residual ratio of Li_2O_2 decreased to 47% after 3 h of charging with X-ray irradiation. In contrast, the XRD pattern of Li_2O_2 -based electrode after 3 h of charging without X-ray irradiation (Fig. 1(b, III)) showed only a slight reduction in Li_2O_2 peaks as compared to the as prepared cell (Fig. 1(b, I)). This corresponded to an 11% Li_2O_2 which agreed well with the calculated theoretical value (10.2%) from the charging capacity of the cell (i.e. pure electrochemical decomposition), which suggests that the Li_2O_2 decomposition is the main reaction during the charging process in our study. The results confirm that X-ray irradiation promotes the electrochemical decomposition of Li_2O_2 during the charging process of the cell.

The relationship between the X-ray intensity and the decomposition rate of Li_2O_2

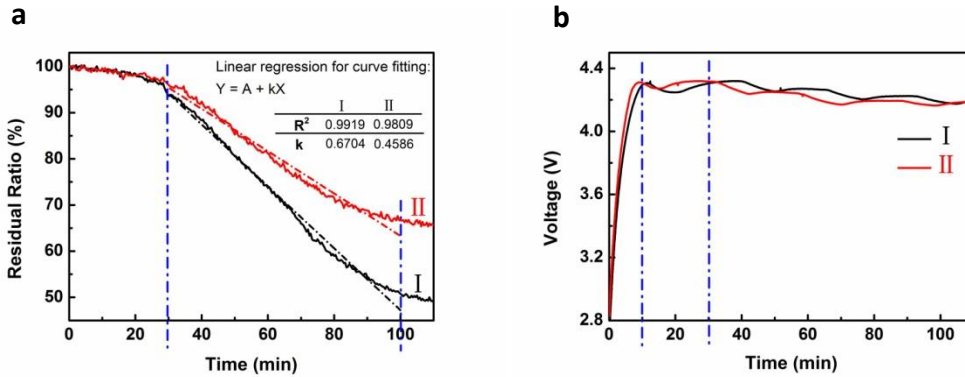


Figure 2.(a) The curves (—) and linear curve fittings (---) of Li_2O_2 decomposition in the electrode charged at a constant current under X-ray irradiation with different intensities (I) I_a , and (II) I_b ($I_b = 68\%$ of I_a), and (b) the charging curves of both cells.

In an attempt to further understand this phenomenon, the effect of X-ray intensity was examined by inserting Al filters in the path of the incident beam. From Fig. 2(a), it can be seen that after 110 min of charging, the residual ratio of Li_2O_2 reduced to 49% with I_a and 66% with I_b ($I_b = 68\%$ of I_a), respectively, which indicates that the intensity of X-ray irradiation does influence on the rate of Li_2O_2 decomposition. The oscillating charging curves shown in Fig. 2(b) maybe caused by the influence of magnetism and/or fluctuant temperature in SR-PXD room. It is noted that no significant difference between the charging curves for both experiments are observed, and this is reasonable given that the X-ray spot only illuminated less than 0.5% of the total area of the electrode under test. The shape of charging profile further indicates that Li_2O_2 decomposition should be the main reaction during the charging plateau, where there are few side reactions including electrolyte decomposition.²⁷ The XRD patterns show that there is little Li_2O_2 decomposition during the initial sloping region upon charging (about the first 10 min charging),

which might be attributed predominantly to double layer charging of the large carbon surface. Interestingly, once a steady potential of 4.2 V was established, a sluggish decomposition of Li_2O_2 during the next 20 min of charging was observed (to be discussed later), which was similar with previously published work.¹⁶ Generally speaking, no obvious enhancement by X-ray in the rate of Li_2O_2 decomposition was observed during the first 30 min of charging.

The X-ray intensity largely affected the electrochemical decomposition of Li_2O_2 after 30 min of charging. After 30 min, the Li_2O_2 decomposition occurs approximately linearly with respect to time ($30 \text{ min} \leq t \leq 100 \text{ min}$), as seen in Fig. 2(a). During this period, *pseudo-zero-order* kinetics was assumed to calculate the corresponding decomposition rate constant k :

$$W = W_0 - kt \quad (1)$$

Where W_0 and W are the original amount of Li_2O_2 before charging, and the residual amount of Li_2O_2 (g) at the charging time t (min), respectively, and k ($\text{g}\cdot\text{min}^{-1}$) is the zero-order decomposition rate constant. The decomposition rate constant under the irradiation I_b ($k_b = 0.4586 \text{ g}\cdot\text{min}^{-1}$) is 68.4% of that under the irradiation I_a ($k_a = 0.6704 \text{ g}\cdot\text{min}^{-1}$). This ratio is almost equal to the ratio (68%) of their respective X-ray intensities ($I_a/I_b \approx k_a/k_b$). This means a proportional relationship exists between the X-ray intensity and the decomposition rate constant. Pure electrochemical decomposition (i.e. non-X-ray effect) in both cases made a contribution to the slight variation in this proportionality.

The effect of the external potential on the electrochemical decomposition of Li_2O_2 under X-ray irradiation

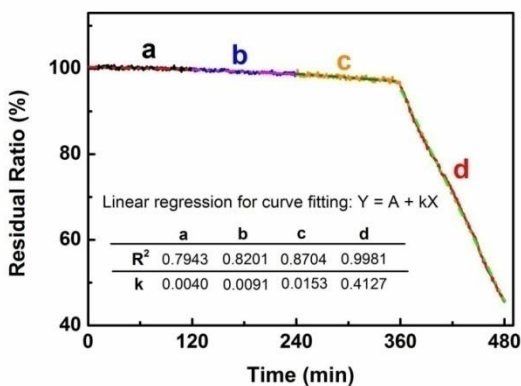


Figure 3. The curves (—) and linear curve fittings (---) of Li_2O_2 decomposition in the electrode charged at a stepwise potential of (a) 3.0 V, (b) 3.4 V, (c) 3.8 V, and (d) 4.2 V.

In order to distinguish our findings from photolysis (i.e. beam damage), the effect of the external potential on the decomposition of Li_2O_2 under X-ray irradiation was investigated by charging one cell at a stepwise potential from 3.0 V to 4.2 V for 120 min at each potential under a constant intensity of X-ray irradiation, as shown in Fig.3. Zero-order kinetics of Li_2O_2 decomposition does also apply here when the cell was charged at constant potentials. In fact, only 0.3%, 1.2% and 2.6% of Li_2O_2 decomposed at the charge voltages of 3.0 V, 3.4 V and 3.8 V during 120 min of charging, respectively. However, when the cell was held at a potential of 4.2 V for 120 min of charging, more than 50% of Li_2O_2 was decomposed, which is 40 times faster than that charged at the same potential without X-ray irradiation (Fig. S2(b) in SI). The big difference between the decomposition rate constants at different potentials demonstrates that X-ray acceleration was observable only when a certain external potential provided, which may be attributed to some steps involved requiring a certain energy barrier. From these results, it has been well established that both X-ray and external potential play important roles in the fast electrochemical decomposition of Li_2O_2 .

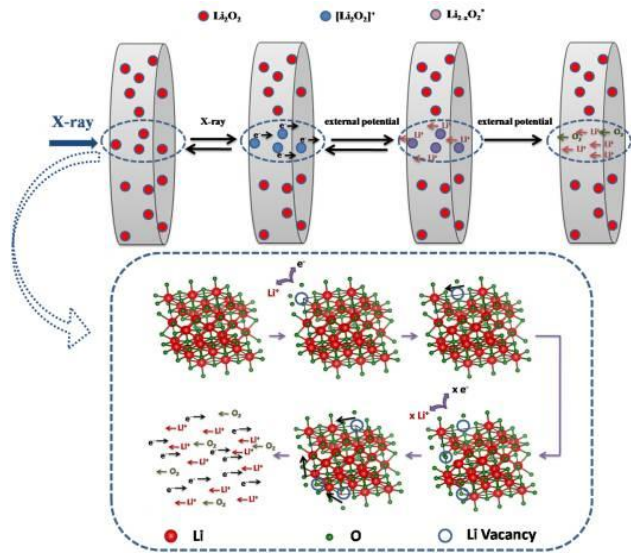


Figure 4. Scheme illustrating the electrochemical decomposition of Li_2O_2 under the X-ray irradiation.

Based on our observations a possible process to describe the X-ray accelerated, electrochemical decomposition is proposed by the following equations:



In the first step, the X-rays eject photo electrons from the Li_2O_2 crystals to form a partly positive species, $[\text{Li}_2\text{O}_2]^{x+}$. From the experimental results, the higher intensity of X-ray can produce more $[\text{Li}_2\text{O}_2]^{x+}$, resulting in a faster decomposition. Therefore, this step can be considered as a kinetically limiting step. Note that the external potential here is also important for driving these free electrons to the counter electrode. Without the external potential, these electrons can recombine quickly with $[\text{Li}_2\text{O}_2]^{x+}$. Ma et al. revealed that X-ray illumination can eject the electrons from a substance, but it cannot complete the electrochemical process.²⁸ In order to keep electric neutrality, $[\text{Li}_2\text{O}_2]^{x+}$ can lose some Li^+ and transform into Li_2O_2 with some Li vacancies

($\text{Li}_{2-x}\text{O}_2^*$) in the second step. Ong et al. demonstrated that the formation energies of a Li vacancy in an intralayer and interlayer of Li_2O_2 are 3.8 eV and 4.1 eV, respectively.²⁹ In other words, a certain driving force is required for the formation of $\text{Li}_{2-x}\text{O}_2^*$, which is in agreement with our results. The moveable Li vacancy can pin into Fermi level at the top of anti-bonding peroxide $\pi^*(2p_x)$ and $\pi^*(2p_y)$ levels in the valance band, leading to an enhanced electronic conductivity of $\text{Li}_{2-x}\text{O}_2^*$,³⁰ which will promote the $\text{Li}_{2-x}\text{O}_2^*$ decomposition, especially at a high rate of charging.³¹ During this step, surface Li^+ can be preferentially released from $[\text{Li}_2\text{O}_2]^{x+}$ into the electrolyte to form $\text{Li}_{2-x}\text{O}_2^*$ with surface Li vacancies. Then, the inner Li atoms can diffuse to the surface Li vacancies, since the diffusion energy is low about 0.36 eV.³² In the last step, the crystal structure of $\text{Li}_{2-x}\text{O}_2^*$ completely collapses to yield Li^+ and O_2 . The energy for the decomposition of $\text{Li}_{2-x}\text{O}_2^*$ and release of O_2 is provided by the external potential during this step. From the beginning of the reaction, the amount of the intermediates ($[\text{Li}_2\text{O}_2]^{x+}$ and $\text{Li}_{2-x}\text{O}_2^*$) gradually increase, and it might take some time to achieve the steady-states of these intermediates before a breakdown of Li_2O_2 framework, which could explain the sluggish decomposition of Li_2O_2 at the early stage. It can be deduced that the external potential contributes to all three steps involved, and a potential threshold might exist in the second and/or last step. In summary, X-ray increases the kinetics of the rate-determining reaction (the first step), while the external potential meets the thermodynamics requirements in the second and/or last steps. The mechanism of X-ray acceleration effect on the Li_2O_2 electrochemical decomposition is proposed by the scheme in Fig. 4.

Finally, this process can be considered similar to light induced electrochemical etching³³ and lithography.³⁴ However, the resolution of these techniques is limited by the wavelength of light source used (normally, UV or visible light). Therefore, it can be expected that X-ray induced

electrochemical etching and lithography would achieve a considerably higher resolution, which could make a significant contribution in the microelectronic industry.³⁵

In summary, for the first time, the accelerating effect of X-rays on the electrochemical decomposition of Li_2O_2 was explored by *operando* SR-PXD. An X-ray acceleration mechanism was proposed based on the experimental results. The conclusion obtained is: (i) X-ray, as a photo energy, accelerates the electrochemical decomposition of Li_2O_2 ; (ii) the electrochemical decomposition of Li_2O_2 under X-ray irradiation follows a zero-order reaction during the main period; (iii) the rate of Li_2O_2 decomposition is proportional to the intensity of X-ray used; (iv) the electrochemical decomposition of Li_2O_2 under X-ray irradiation may involve a three-step reaction with $[\text{Li}_2\text{O}_2]^{\text{x}+}$ and $\text{Li}_{2-\text{x}}\text{O}_2^*$ as intermediates; and (v) The X-ray interaction promotes kinetics, while the external potential overcomes the thermodynamic barriers. The findings here indicate that there could be other routes than a single-step reaction for Li_2O_2 electrochemical decomposition in Li- O_2 battery. If some way (e.g. by electrocatalysts) to induce the ionization of Li_2O_2 and/or enhance its conductivity could be adopted, an accelerated charging process can be expected, and the selectivity will be consequently improved due to the overwhelming kinetics of the main reaction, Li_2O_2 decomposition. High-resolution electrochemical etching could be achieved with the assistance of X-ray irradiation, and the etching speed could be tuned by X-ray intensity. This advance could be applied in the microelectronics industry.

Experimental Methods

a. Li_2O_2 -based electrode preparation and the electrochemical cell assembly. The porous Li_2O_2 -based positive electrodes consisted of Super P carbon (lithium battery grade, ErachemComilog), Kynar 2801 (a copolymer based on PVDF, Arkema), Li_2O_2 powder (technical grade, 90%, Sigma-Aldrich) and silicon (99.5%, Alfa Aesar) in weight ratio of

48:7:35:10. Silicon was added as an inert internal reference to calculate the amount of Li_2O_2 present in a given sample, since it provides stable and strong diffraction peaks in the XRD patterns. Super P carbon, Li_2O_2 and silicon were mixed by high energy ball-milling in a coffee bag for 1 h. To the mixture, Kynar binder and acetone ($\geq 99.0\%$, Fluka) were added to prepare a slurry, which was hand-milled for 30 min. The slurries were cast drop wise onto an aluminum mesh with a diameter of 1.3 cm and a flat area of 1.32 cm^2 . The acetone was then left to evaporate, and the electrodes were further dried at $120 \text{ }^\circ\text{C}$ for 5 h in a vacuum (Buchi Glass Oven B-585). All the operations were performed in an Ar-filled glove box (H_2O and $\text{O}_2 < 1 \text{ ppm}$). The electrode construction is similar with that of a cathode in a Li- O_2 cell.³⁶

All the electrochemical cells were assembled in an Ar-filled glove box using a pouch cell (i.e. “coffee bag” cell) with the following components: Li foil negative electrode, double-layer Solupor separator soaked in electrolyte (1 M LiPF_6 in PC, Ferro, Purolyte), and porous Li_2O_2 -based positive electrode described above (Fig. S3(a) in SI).

b. *Operando* SR-PXD measurement. *Operando* SR-PXD (measuring the synchrotron-based XRD during the charging process of a cell) was conducted using beamline I711 at the MAX II synchrotron of Max IV Laboratory in Lund, Sweden (Figs. S3(b-d) in SI).³⁷ The cells were mounted in transmission mode, and an Oxford diffraction Titan CCD was used to collect diffraction pattern. Lanthanum hexaoride (LaB_6 , SRM-660) was used as a reference material to calibrate the different parameters of powder diffraction instrument (wavelength, sample-to-detector distance and tilt angle). The refined X-ray wavelength was 0.991 \AA . During a standard experiment, the frames were collected under continuous X-ray irradiation (an exposure time of 20 s was used to collect a single frame, followed by a 5 s dark period during the detector read out). A frame is the integrated data collected on the detector during the exposure. This data was

later converted to an intensity vs. 2θ plot, through circular integration. The diameter of X-ray irradiation spot was about 0.8 mm. To adjust the X-ray intensity, Al filters were employed. Initially, a few frames were collected in the absence of any charging current. This was then followed by the collection of further frames in an *operando* mode, i.e. during charging the cells using an external potentiostat (SP-240, Bio-Logic SAS) at a constant current of $40 \text{ mA}\cdot\text{g}^{-1}$ from open circuit voltage (OCV) to 4.5 V. Data were also collected while one cell was charged under stepwise potentiostatic control from 3.0 V to 4.2 V for periods of 120 min at each potential under the X-ray irradiation with the constant intensity. The program Fit2D was used to integrate the 2D diffraction images,³⁸ and the FullProf program was employed to refine the XRD patterns and analyze the weight fraction of Li_2O_2 and Si.³⁹ The residual ratio of Li_2O_2 in each cell during the charging process was calculated from eq. S1 in SI.

c. In house *in situ* X-ray diffraction measurement. In order to study the electrochemical decomposition of Li_2O_2 without the influence of X-ray irradiation, in house *in situ* XRD analysis (XRD measurement of the whole cell without unpacking it before and after the charging process) was also performed in transmission mode using a STOE diffractometer with a position-sensitive detector and Co $K\alpha$ radiation ($\lambda = 1.789 \text{ \AA}$), operating at 45 kV and 32 mA. The residual ratio of Li_2O_2 in each cell charged at a constant current or constant potential was calculated, based on eq. S1 in SI as well.

ASSOCIATION CONTENT

Supporting Information. The curve of Li_2O_2 decomposition in the electrode with the same amount of Li_2O_2 where no charging current was applied under constant X-ray irradiation for 8 h, *in situ* XRD patterns of a Li_2O_2 -based electrode before charging and after 10 h charging, images

of a cell sealed in a coffee bag and SR-XRD, schematic diagram of the beamline I711, and the formula for calculating the residual ration of Li_2O_2 in each cell during charging process. This material is available free of charge via the Internet at <http://pubs.acs.org>.

AUTHOR INFORMATION

Corresponding Author

*E-mail: jiefang.zhu@kemi.uu.se

Notes

The authors declare no competing financial interests.

ACKNOWLEDGMENT

This work was financially supported by Swedish Research Council, Swedish Energy Agency, Ångpanneföreningen's Foundation for Research and Development, and J. Gust. Richert Foundation. We also acknowledge the support from the MAX IV Laboratory for using synchrotron radiation powder X-ray diffraction.

REFERENCES

1. McDevitt, J. T. Photoelectrochemical solar cells. *J. Chem. Educ.* **1984**, *61* (3), 217-221.
2. Fujishima, A.; Honda, K. Electrochemical photolysis of water at a semiconductor electrode. *Nature* **1972**, *238* (5358), 37-38.
3. Gratzel, M. Photoelectrochemical cells. *Nature* **2001**, *414* (6861), 338-344.
4. Pearson, A.; Jani, H.; Kalantar-zadeh, K.; Bhargava, S. K.; Bansal, V. Gold nanoparticle-decorated keggin ions/ TiO_2 photococatalyst for improved solar light photocatalysis. *Langmuir* **2011**, *27* (11), 6661-6667.
5. Alpatova, N. M.; Krishtalik, L. I.; Pleskov, Y. V. Electrochemistry of solvated electrons. In *Organolithium Compounds/Solvated Electrons*, Springer Berlin Heidelberg: 1987; Vol. 138, pp 149-219.

6. Shao, Y.; Park, S.; Xiao, J.; Zhang, J.-G.; Wang, Y.; Liu, J. Electrocatalysts for nonaqueous lithium-air batteries: Status, challenges, and perspective. *ACS Catalysis* **2012**, *2* (5), 844-857.
7. Younesi, R.; Hahlin, M.; Treskow, M.; Scheers, J.; Johansson, P.; Edström, K. Ether based electrolyte, LiB(CN)₄ salt and binder degradation in the Li-O₂ battery studied by hard X-ray photoelectron spectroscopy (HAXPES). *The Journal of Physical Chemistry C* **2012**, *116* (35), 18597-18604.
8. Freunberger, S. A.; Chen, Y.; Peng, Z.; Griffin, J. M.; Hardwick, L. J.; Barde, F.; Novak, P.; Bruce, P. G. Reactions in the rechargeable lithium-O₂ battery with alkyl carbonate electrolytes. *J. Am. Chem. Soc.* **2011**, *133* (20), 8040-8047.
9. McCloskey, B. D.; Bethune, D. S.; Shelby, R. M.; Girishkumar, G.; Luntz, A. C. Solvents' critical role in nonaqueous lithium-oxygen battery electrochemistry. *The Journal of Physical Chemistry Letters* **2011**, *2* (10), 1161-1166.
10. Younesi, R.; Hahlin, M.; Roberts, M.; Edström, K. The SEI layer formed on lithium metal in the presence of oxygen: A seldom considered component in the development of the Li-O₂ battery. *Journal of Power Sources* **2013**, *225*, 40-45.
11. Assary, R. S.; Lu, J.; Du, P.; Luo, X.; Zhang, X.; Ren, Y.; Curtiss, L. A.; Amine, K. The effect of oxygen crossover on the anode of a Li-O₂ battery using an ether-based solvent: Insights from experimental and computational studies. *ChemSusChem* **2013**, *6* (1), 51-55.
12. Peng, Z.; Freunberger, S. A.; Chen, Y.; Bruce, P. G. A reversible and higher-rate Li-O₂ battery. *Science* **2012**, *337* (6094), 563-566.
13. Oh, S. H., Black, R., Pomerantseva, E., Lee, J-H and Nazar, L.F. Synthesis of a metallic mesoporous pyrochlore as a catalyst for lithium-O₂ batteries. *Nature chemistry* **2012**, *4*, 1004-1010.
14. Gallant, B. M.; Mitchell, R. R.; Kwabi, D. G.; Zhou, J.; Zuin, L.; Thompson, C. V.; Shao-Horn, Y. Chemical and morphological changes of Li-O₂ battery electrodes upon cycling. *The Journal of Physical Chemistry C* **2012**, *116* (39), 20800-20805.
15. Black, R.; Oh, S. H.; Lee, J.-H.; Yim, T.; Adams, B.; Nazar, L. F. Screening for superoxide reactivity in Li-O₂ batteries: Effect on Li₂O₂/LiOH crystallization. *J. Am. Chem. Soc.* **2012**, *134* (6), 2902-2905.
16. Lim, H.; Yilmaz, E.; Byon, H. R. Real-time XRD studies of Li-O₂ electrochemical reaction in nonaqueous lithium-oxygen battery. *The Journal of Physical Chemistry Letters* **2012**, *3* (21), 3210-3215.
17. Jung, H.-G., Hassoun, J., Park J-B., Sun, Y-K. and Scrosati, B. An improved high-performance lithium-air battery. *Nature chemistry* **2012**, *4*, 579-585.
18. Laoire, C. O.; Mukerjee, S.; Plichta, E. J.; Hendrickson, M. A.; Abraham, K. M. Rechargeable lithium/TEGDME-LiPF₆/O₂ battery. *Journal of The Electrochemical Society* **2011**, *158* (3), A302-A308.
19. Ryan, K. R.; Trahey, L.; Okasinski, J. S.; Burrell, A. K.; Ingram, B. J. In situ synchrotron X-ray diffraction studies of lithium oxygen batteries. *Journal of Materials Chemistry A* **2013**, *1* (23), 6915-6919.
20. Shui, J. L.; Okasinski, J. S.; Kenesei, P.; Dobbs, H. A.; Zhao, D.; Almer, J. D.; Liu, D. J. Reversibility of anodic lithium in rechargeable lithium-oxygen batteries. *Nature communications* **2013**, *4*, 2255.

21. Shui, J. L.; Okasinski, J. S.; Zhao, D.; Almer, J. D.; Liu, D. J. Microfocused X-ray study on precipitate formation in the separator region of nonaqueous Li-O₂ batteries. *ChemSusChem* **2012**, *5* (12), 2421-6.
22. Veith, G. M.; Dudney, N. J.; Howe, J.; Nanda, J. Spectroscopic characterization of solid discharge products in Li-air cells with aprotic carbonate electrolytes. *The Journal of Physical Chemistry C* **2011**, *115* (29), 14325-14333.
23. Younesi, R.; Urbonaite, S.; Edström, K.; Hahlin, M. The cathode surface composition of a cycled Li-O₂ battery: A photoelectron spectroscopy study. *The Journal of Physical Chemistry C* **2012**, *116* (39), 20673-20680.
24. Younesi, R.; Hahlin, M.; Edstrom, K. Surface characterization of the carbon cathode and the lithium anode of Li-O₂ batteries using LiClO₄ or LiBOB salts. *ACS applied materials & interfaces* **2013**, *5* (4), 1333-1341.
25. Ryan, K. R.; Trahey, L.; Ingram, B. J.; Burrell, A. K. Limited stability of ether-based solvents in lithium-oxygen batteries. *The Journal of Physical Chemistry C* **2012**, *116* (37), 19724-19728.
26. Qiao, R.; Chuang, Y.-D.; Yan, S.; Yang, W. Soft X-Ray irradiation effects of Li₂O₂, Li₂CO₃ and Li₂O revealed by absorption spectroscopy. *PLoS One* **2012**, *7* (11), e49182.
27. Lu, Y.-C.; Shao-Horn, Y. Probing the reaction kinetics of the charge reactions of nonaqueous Li-O₂ batteries. *The Journal of Physical Chemistry Letters* **2013**, *4* (1), 93-99.
28. Ma, Q.; Divan, R.; Mancini, D. C.; Rosenberg, R. A.; Quintana, J. P.; Keane, D. T. X-ray induced, substrate-carrier mediated deposition of metal on GaAs. *Applied Physics Letters* **2006**, *89* (8), 083114.
29. Ong, S. P.; Mo, Y.; Ceder, G. Low hole polaron migration barrier in lithium peroxide. *Physical Review B* **2012**, *85* (8), 081105.
30. Hummelshøj, J. S.; Blomqvist, J.; Datta, S.; Vegge, T.; Rossmeisl, J.; Thygesen, K. S.; Luntz, A. C.; Jacobsen, K. W.; Nørskov, J. K. Communications: Elementary oxygen electrode reactions in the aprotic Li-air battery. *J. Chem. Phys.* **2010**, *132* (7), 071101.
31. Zhong, L.; Mitchell, R. R.; Liu, Y.; Gallant, B. M.; Thompson, C. V.; Huang, J. Y.; Mao, S. X.; Shao-Horn, Y. In situ transmission electron microscopy observations of electrochemical oxidation of Li₂O₂. *Nano Lett* **2013**, *13* (5), 2209-14.
32. Chen, J.; Hummelshøj, J. S.; Thygesen, K. S.; Myrdal, J. S. G.; Nørskov, J. K.; Vegge, T. The role of transition metal interfaces on the electronic transport in lithium-air batteries. *Catalysis Today* **2011**, *165* (1), 2-9.
33. Ma, Q.; Moldovan, N.; Mancini, D. C.; Rosenberg, R. A. Wet etching of GaAs using synchrotron radiation x rays. *Journal of Applied Physics* **2001**, *89* (5), 3033.
34. Wang, X.; Zhang, D.; Chen, Y.; Zhu, L.; Yu, W.; Wang, P.; Yao, P.; Ming, H.; Wu, W.; Zhang, Q. Large area sub-wavelength azo-polymer gratings by waveguide modes interference lithography. *Applied Physics Letters* **2013**, *102* (3), 031103.
35. Eliseev, A. A.; Sapoletova, N. A.; Snigireva, I.; Snigirev, A.; Napolskii, K. S. Electrochemical X-ray photolithography. *Angew. Chem. Int. Ed. Engl.* **2012**, *51* (46), 11602-5.
36. Xu, W.; Viswanathan, V. V.; Wang, D.; Towne, S. A.; Xiao, J.; Nie, Z.; Hu, D.; Zhang, J.-G. Investigation on the charging process of Li₂O₂-based air electrodes in Li-O₂ batteries with organic carbonate electrolytes. *Journal of Power Sources* **2011**, *196* (8), 3894-3899.
37. Cerenius, Y.; Ståhl, K.; Svensson, L. A.; Ursby, T.; Oskarsson, Å.; Albertsson, J.; Liljas, A. The crystallography beamline I711 at MAX II. *Journal of Synchrotron Radiation* **2000**, *7* (4), 203-208.

38. Hammersley, A. P.; Svensson, S. O.; Hanfland, M.; Fitch, A. N.; Hausermann, D. Two-dimensional detector software: From real detector to idealised image or two-theta scan. *High Pressure Research* **1996**, *14* (4-6), 235-248.
39. Rodriguez-Carvajal, J. Fullprof, program for rietveld refinement, version 3.7. *LLB JRC* **1997**.